analytical chemistry

pubs.acs.org/ac Article

Ultra-Trace Protein Detection by Integrating Lateral Flow Biosensor with Ultrasound Enrichment

Yan Huang, Tailin Xu,* Yong Luo, Conghui Liu, Xuan Gao, Zhihao Cheng, Yongqiang Wen, and Xueji Zhang*

Cite This: *Anal. Chem.* 2021, 93, 2996−3001 Read Online

ACCESS | Metrics & More | Article Recommendations | Supporting Information

ABSTRACT: Lateral flow biosensor (LFB) is one of the most successful and applied commercial detection methods for food safety, drug abuse, and disease. Here, we integrated the ultrasound enrichment as sample preparation with LFB to achieve the ultra-trace protein detection in blood. When the ultrasound field is applied, the interaction between the acoustic field and gold nanoparticles can gather specifically modified gold nanoparticles toward pressure nodes in seconds and enrich target proteins. Such an approach can detect protein with a linear range of 1−20 ng mL^{-1} and detection limit of 0.58 ng mL^{-1} in blood within 20 min, which enormously reduces false positive readings caused by interference in real blood samples with complex components. Such a microchip that integrated acoustic enrichment with LFB shows great potential in detecting ultra-trace biomarkers for clinical diagnosis.

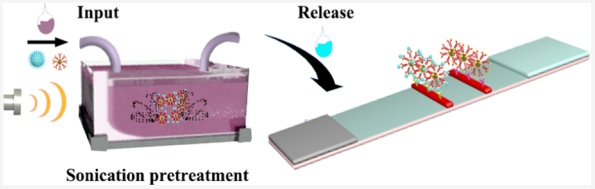

INTRODUCTION

Point-of-care tests (POCTs) and in field-rapid diagnostic tests are of great significance in early detection.[1−6] Lateral flow biosensor (LFB), the invention of which can be tracked back to the early 1980s,[7] is one of the most important representatives in ultra-trace analysis with the distinguishing features of simplicity, rapidness, and cost-effectiveness,[8−12] which have been used as commercial products for POCT screening of pregnancy, infectious diseases, and drug abuse.[11] However, the LFBs have been criticized for their limited ability of detection in complex real samples, thus much efforts still need to be devoted to pre-handle the body fluids (e.g., blood, urine, and sweat) for the purpose of getting rid of interfering components and improving the detection ability of LFBs.[13−15]

Sample pre-treatment is an important part for the LFB to achieve ultra-trace detection in real samples. In the early studies, membrane filtration and electrophoresis are often used for the enrichment and separation of targets from complex samples. Materials such as nylon,[16] nitrocellulose (NC) membranes,[17,18] glass fiber,[17] hydrogel,[23] and whole blood separation membrane[18] have been used as filters to pretreat oral fluids,[16] drinking water samples,[17] serum,[19] lysed blood,[20] and whole blood[18] in the LFBs. In the last 10 years, magnetic separation as a convenient method has been widely used as a sample pretreatment approach to separate bacterial or protein biomarkers from the complex matrix such as blood, milk, and cytosol.[21−26] Recently, ultrasound actuation with swarming or assembling behavior[27] exhibits excellent ability of regulating nanoparticles[28−31] and has a profound impact upon diverse applications such as propelling nanowires and manipulating cells.[32−38] Last year, our group integrated the ultrasound pre-treatment approach with surface-enhanced Raman scattering[39] and fluorescence[40] to achieve ultra-trace detection of nucleic acids. Compared with magnetic or other separation methods, ultrasound pre-treatment responds quickly (just in seconds), disregards the morphology or size of particles, and is easy to control, thus providing an opportunity as a pre-treatment approach to integrate LFBs to enrich and detect ultra-trace biomarkers for clinical diagnosis.

Herein, we first introduced the ultrasound enrichment as a new pretreatment method to achieve sample preparation for LFBs. On such an integrated platform, antibody-labeled gold nanoparticle (GNP) was adopted as a carrier to capture target protein. Under the simulation of ultrasound, the GNPs can be enriched to the ultrasound pressure node, which also resulted in enriching rabbit IgG. After washing under ultrasound state, the GNP−antibody−protein complex was transferred to the LFB for detection. Our results showed that, after enrichment, the integrated LFB device can detect a linear range of 1−20 ng mL^{-1} for rabbit IgG in blood. Such platform-integrated ultrasound separation with the LFB shows great potential in developing an on-chip detection platform for clinical POCTs.

Received: November 30, 2020
Accepted: January 21, 2021
Published: January 29, 2021

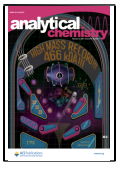

Downloaded via BUTLER UNIV on May 15, 2021 at 04:34:53 (UTC).
See https://pubs.acs.org/sharingguidelines for options on how to legitimately share published articles.

ACS Publications © 2021 American Chemical Society

https://dx.doi.org/10.1021/acs.analchem.0c05032
Anal. Chem. 2021, 93, 2996−3001

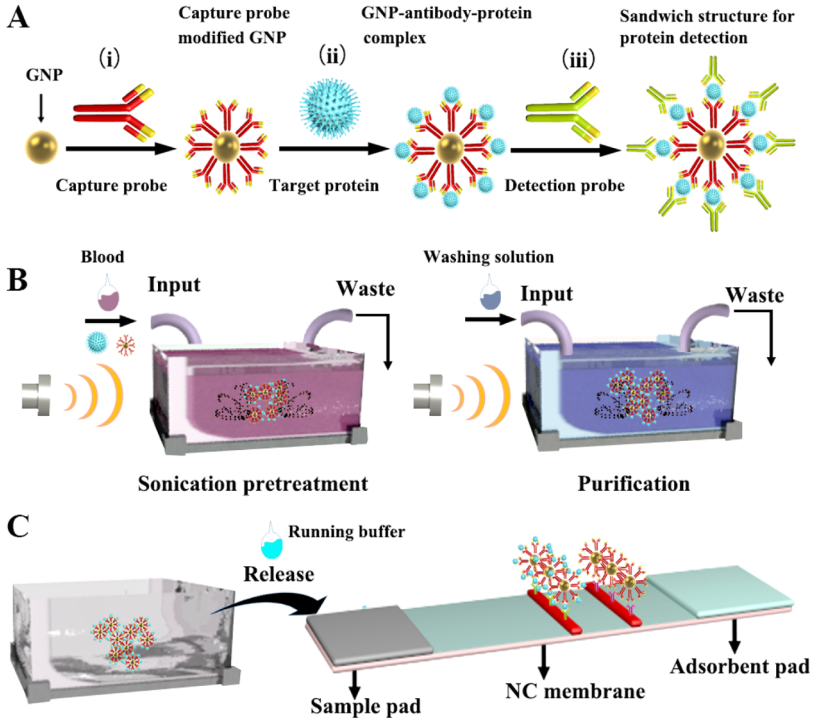

Figure 1. Principle of protein detection by integrating ultrasound pretreatment with LFB. (A) Schematic of identification and detection of target protein by GNP-labeled antibody. (B) Enrichment and purification of target protein by ultrasound pretreatment. (C) Releasing the GNP−antibody−target complex and detecting on LFB.

EXPERIMENTAL SECTION

Fabrication of Ultrasound-Integrated LFB Platform. *LFB Fabrication.* GNP−antibody conjugates were prepared according to the reported methods with slight modifications, that is, the antibody was changed to goat anti-Rabbit IgG.[21] LFBs were manufactured according to the reported methods.[22]

Description of Ultrasonic Device. The ultrasound device was similar to the method previously reported.[39] The piezoelectric transducer was bonded to the bottom of the reaction cavity through a conductive gel, and an arbitrary waveform generator and a homemade power amplifier were connected in series. The arbitrary waveform generator generated a sine wave, which was amplified by the power amplifier and then transmitted to the piezoelectric transducer to generate ultrasonic waves. Correspondingly, ultrasonic waves superimposed in the reaction cavity to form acoustic pressure nodes and drive the aggregation of the GNP−antibody and GNP−antibody−protein complex.

Analysis Procedure. GNP−antibody conjugates and IgG-doped blood were mixed pumped into the cavity with ultrasound. After 5 min, the blood was pumped out with the existence of ultrasound. Then, phosphate-buffered saline (PBS) solution was pumped into the cavity and mixed with the GNP−antibody−IgG complex for the purpose of washing the complex with the absence of ultrasound. The solution was pumped out with the existence of ultrasound. This wash procedure was repeated for three times. Next, a running solution (PBS + 1% bovine serum albumin) was pumped into the cavity, mixed well, and pumped out to the LFB with absence of ultrasound (Figure S3). 10 minutes later, the results were recorded.

RESULTS AND DISCUSSION

Detection Principle of Ultrasound-Integrated LFB. Figure 1 shows the scheme of protein detection by integrating ultrasound pretreatment with LFB. The detailed processes involve ultrasonic enrichment in an ultrasound device, for the pre-separation of protein−antibody−GNP from the complex matrix, and signal detection in a LFB. First, GNP was conjugated with detection antibody. Then, GNP−antibody conjugate was introduced to a reaction cavity to capture and pre-enrich the target protein in complex samples (e.g., blood) (Figure 1A). We mixed the GNP−antibody conjugate into the blood sample. Without an ultrasonic field, the GNPs show common Brownian motion and are uniformly distributed in solution. Next, an arbitrary waveform generator was attached to a radio frequency power amplifier and a piezoelectric transducer waveform generator, to generate continuous acoustic wave. Continuous acoustic wave passed through a steel plate and finally reached the plasma desorption mass spectrometry (PDMS) cavity. The interaction between the ultrasound wave and the PDMS cavity wall and cover glass can result in the differential pressure field. When applying specific frequency and voltage, the GNP can be gathered to the center of the cavity. In this way, the target, captured by the GNP−antibody, in the complex solution can be enriched.

The ultrasound device was turned on after incubation for 5 min, and the GNP−antibody conjugate and GNP−antibody−protein complex from the blood can be collected into the acoustic pressure node area in the cavity. With the existence of ultrasound, the solutions were drained out of the cavity. After the GNP−antibody−protein complex was cleaned by a washing solution, we turned off the ultrasound, resuspended the complex in a running buffer, and detected the sample in the LFB (Figure 1B). The GNP−antibody−protein complex reacted with the capture antibody to form a sandwich structure

https://dx.doi.org/10.1021/acs.analchem.0c05032
Anal. Chem. 2021, 93, 2996−3001

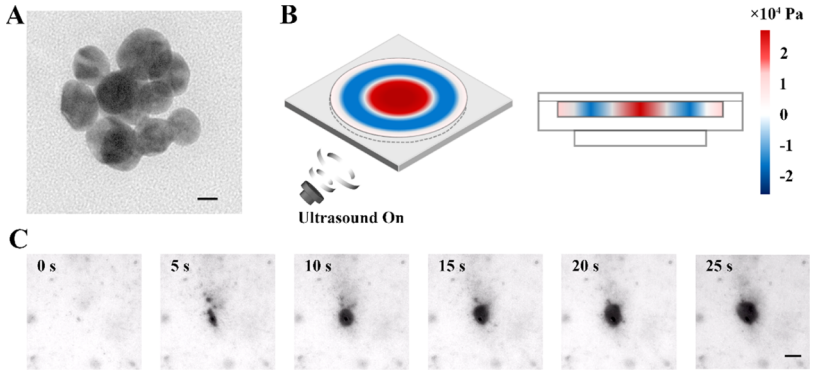

Figure 2. GNP aggregation performing ultrasound. (a) Transmission electron microscope image of the GNPs. Scale bar: 10 nm. (b) Pressure distribution simulation by adjusting the ultrasonic field pressure node to the center of the cavity under specific frequency and pressure conditions. (c) Actual time-lapse microscopic images of aggregation of GNPs (Supporting Information, Video S1). Scale bar: 50 μm; GNP concentration: ~1 × 10^{-8} mol L^{-1}; ultrasound frequency: ~1.7 MHz, voltage 300 mV.

and accumulated to produce a red line on the test zone of the LFB. The uncaptured GNP−antibody and the GNP−antibody−protein complex were fixed on the control zone by the second antibody to produce a second line. In this way, two red lines can be observed. When there is no target protein in the blood, only GNP−antibody existed in the running buffer, resulting in only one line being observed in the LFB. The grayscale of the lines can be obtained by a portable strip reader or a smartphone.

GNP Aggregation in the Ultrasonic Field. To verify the aggregation and dispersion properties of GNP in the ultrasonic field, GNP was first operated in an aqueous solution in a PDMS cavity. In this work, GNP, with an average size of 20 nm (Figure 2a), was used to conjugate with antibodies. The piezoelectric transducer output continuous ultrasonic waves to the reaction cavity when the ultrasound device was turned on. At a fixed acoustic frequency, ultrasonic waves were reflected on the inner wall of the reaction cavity and superimposed to form ultrasonic standing waves, thereby establishing a pressure field on the reaction cavity and generating acoustic pressure nodes.[30,33,41,42] The interaction between the cavity and the ultrasonic pressure field cannot be simply settled by an easy acoustic wave equation because of its complexity, thus we adopted the numerical simulation to assist the design of the micro-cavity to ensure that there is only one pressure node at the center of the PDMS cavity,[31,43] the results of which (oblique view and front view) are shown in Figure 2b. It can be seen that there is one single pressure node at the center of the cavity, indicating that our device can be used for nanoparticle enrichment.

The acoustic radiation force generated by the uneven distribution of ultrasound pressure can drive the nanoparticles to migrate to the acoustic pressure node.[31,44] In our work, the GNPs in the reaction cavity quickly aggregated to the acoustic pressure node under the combined action of acoustic radiation force and acoustic flow. In this way, the target can be enriched with GNPs. Figure 2c shows the time-lapse microscopic images of the collective GNPs. With the application of ultrasound (~1.7 MHz frequency, 300 mV voltage), the GNPs in the solution instantly migrated toward the cavity center, and the red solution started to emerge as a visible aggregate within 5 s. This aggregate does not become larger after 20 s, which means that the ultrasound enrichment of GNPs can be completed within 20 s.

Numerical Simulation of Ultrasound Model. A finite element model was used to simulate the ultrasound pressure distribution in the cavity at certain ultrasonic frequencies. Electrostatics, piezoelectric excitation sound field, and solid mechanics are included in the physics field of this model. The pressure in the liquid domain was assumed to vary harmonically in time. In this way, the wave equation for the ultrasound pressure distribution can be described as

$$\nabla \times \left(-\frac{1}{\rho_0}(\nabla p)\right) - \frac{\omega^2 p}{\rho_0 c_s^2} = 0 \quad (1)$$

In the equation, ω represents the driving frequency of the ultrasound field, p indicates the ultrasound pressure distribution of the aqueous solution, c_s represents the transmission speed in the solution of sound wave, and ρ_0 indicates the solution density.

Next, boundary conditions were added to the model. Because the bottom surface of the piezo transducer prevented the ultrasound pressure distribution from moving along the z-direction, we assigned it to a roller boundary condition. The normal component of the boundary acceleration of the solid (piezoelectric transducer) structure driving the sample reservoir at the interface of the PDMS cavity and the piezoelectric transducer is described in eq 2

$$n \times \left(\frac{1}{\rho_0}(\nabla p)\right) = a_n \quad (2)$$

In the equation, n indicates the normal vector of the outer surface of each individual cell and a_n represents the normal acceleration component of the liquid domain driven by the piezoelectric transducer.

In the light of this model, the sound pressure distribution can be calculated when the ultrasonic excitation frequency was determined, so suitable excitation frequencies for different PDMS sample cell sizes can be found. Once our case is determined, parameters such as ρ_0 and c_s in the formula will not change. Consequently, the sound pressure field distribution can be changed by altering the excitation frequency.[45]

Analysis of Rabbit IgG Doped in Blood using the Ultrasound-Integrated LFB. Rabbit IgG was used for proof of concept. It was doped into blood, and the conjugate GNP−antibody was added for cultivation. First, we compare the detection results with and without ultrasonic separation. The typical photo image and the corresponding gray values of the

https://dx.doi.org/10.1021/acs.analchem.0c05032
Anal. Chem. 2021, 93, 2996−3001

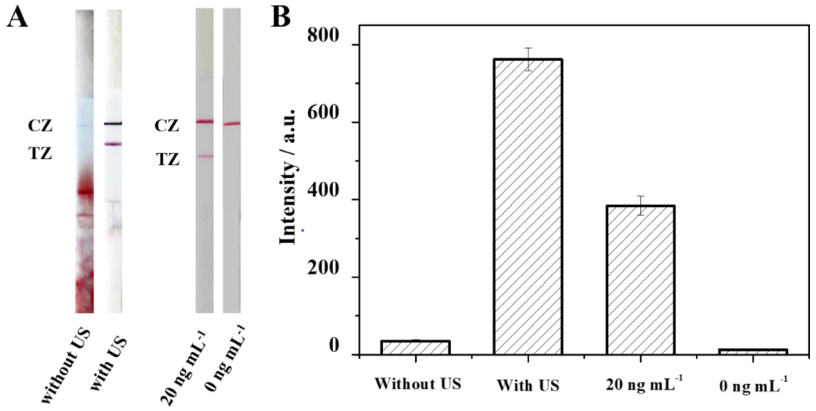

Figure 3. Photo pictures (A) and intensity (B) of LFBs detecting IgG of 200 ng mL^{-1} in blood without and with ultrasound, detecting IgG of 20 and 0 ng mL^{-1} in blood with ultrasound. TZ: test zone, CZ: control zone, US: ultrasound. The value represented by each bar chart is the average of three data.

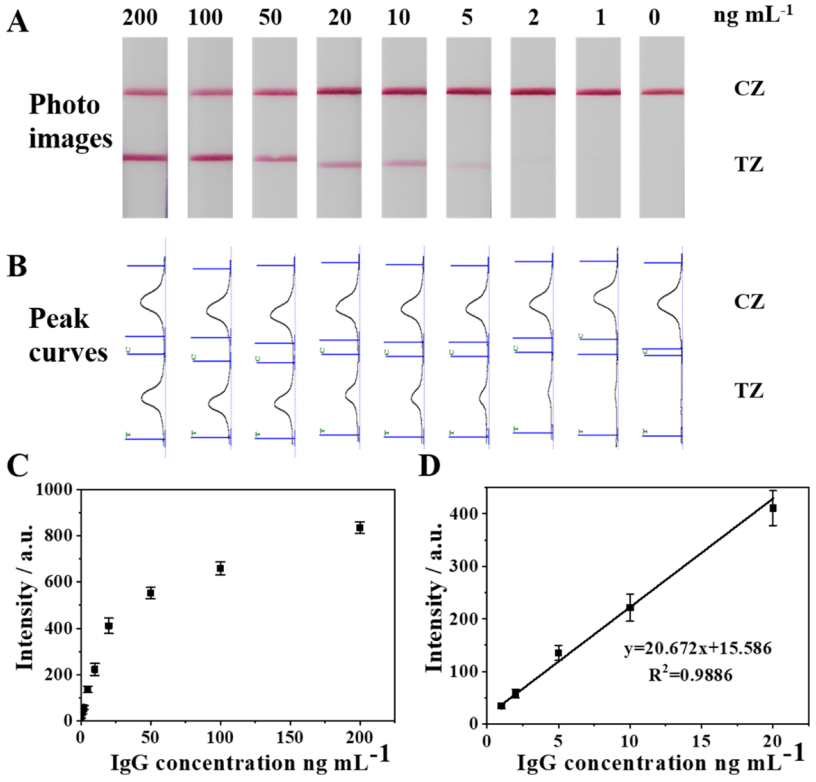

Figure 4. Photo pictures (A) and corresponding peak curves (B) of LFBs with doped rabbit IgG concentration of 0−200 ng mL^{-1}, and the calibration curve (C) and linear range (D) of the ultrasound-integrated LFB device. Each data point is the average of three measurement data.

test zone are shown in Figure 3A and Figure 3B, respectively. As the control group, the blood sample was directly loaded to the LFB. Without ultrasonic separation, the LFB did not run clean and there were many blood cells left on the sample pad and the NC membrane. The test line can be hardly observed. After ultrasonic separation, disturbances such as blood cells and other proteins in the blood were removed. The rest of the complex was redissolved in the buffer solution, so the LFB runs neat and clean and there was a clear red line on the test zone (on the left side of Figure 3A). Then, the feasibility of the ultrasound-integrated LFB was verified by detecting blood doped with 20 ng mL^{-1} IgG protein and the blood without IgG protein after sonication separation (on the right side of Figure 3A). A clear red line can be seen on the test zone of the LFB with rabbit IgG, but no red line showed without target, which proved that the ultrasound-integrated LFB device can detect rabbit IgG in blood.

After parameter optimization (Figure S2), the concentration gradient and linear relationship of the ultrasound-integrated LFB systems was investigated. Figure 4 shows the images of the gradient detection (Figure 4A) and the corresponding grayscale value of the test zone (Figure 4B) on blood doped with 0−200 ng mL^{-1} IgG protein. We can see that the depth of the red color of the line on the test zone increases with the addition of the doped IgG concentration. The grayscale value of the test zone is linear with the IgG concentration in 1−20 ng mL^{-1}, and the visual detection limit of rabbit IgG protein in blood was 0.58 ng mL^{-1}. The above experiments prove that ultrasonic treatment can separate specific proteins in complex matrices. It does not require special nanomaterials such as

https://dx.doi.org/10.1021/acs.analchem.0c05032
Anal. Chem. 2021, 93, 2996−3001

magnetic nanomaterials, and commonly used nanogold can be separated. It has important potential for practical detection of proteins in complex matrices. Then, we used the ultrasound-integrated LFB to detect the IgG in blood doped with 0, 2, and 20 ng mL^{-1} for six times, and the relative standard deviations of the six sets of data were 2.28, 8.32, and 9.70%, respectively, indicating good reproducibility (Table S1). In addition, the detection of other doped proteins at the same concentration shows that our ultrasound-integrated LFB has good selectivity (Figure S3).

CONCLUSIONS

Ultrasound enrichment, as a sample pretreated method, was for the first time integrated with LFB to develop a rapid and universal platform for protein detection in blood. Unlike magnetic separation that requires magnetic nanoparticles, conventional nanoparticles (such as GNPs) can be used for ultrasonic pretreatment. By introducing ultrasonic waves in the liquid cavity, controlled aggregation and dispersion of GNP can be achieved. This GNP enrichment ability is remarkably effective for protein separation and detection in blood. Besides, changing the antibody attached to GNPs by the deoxyribonucleic acid probe, this platform can also be used to detect nucleic acids. Our work sets off a new approach for pretreatment in LFBs and has great potential in future POCTs in different kinds of areas like hazardous substance detection, food safety, early disease detection, and epidemic outbreak surveillance.

ASSOCIATED CONTENT

Supporting Information

The Supporting Information is available free of charge at https://pubs.acs.org/doi/10.1021/acs.analchem.0c05032.

Experimental section, flow chart of the integrated LFB system, reproducibility, parameter optimization, and selectivity of the LFB (PDF)

Actual time-lapse microscopic images of aggregation of GNPs (MPG)

AUTHOR INFORMATION

Corresponding Authors

Tailin Xu − *Beijing Key Laboratory for Bioengineering and Sensing Technology, School of Chemistry and Biological Engineering, University of Science and Technology Beijing, Beijing 100083, P. R. China; School of Biomedical Engineering, Shenzhen University, Shenzhen, Guangdong 518060, P. R. China;* orcid.org/0000-0003-4037-2856; Email: xutailin@ustb.edu.cn

Xueji Zhang − *Beijing Key Laboratory for Bioengineering and Sensing Technology, School of Chemistry and Biological Engineering, University of Science and Technology Beijing, Beijing 100083, P. R. China; School of Biomedical Engineering, Shenzhen University, Shenzhen, Guangdong 518060, P. R. China;* orcid.org/0000-0002-0035-3821; Email: zhangxueji@ustb.edu.cn

Authors

Yan Huang − *Beijing Key Laboratory for Bioengineering and Sensing Technology, School of Chemistry and Biological Engineering, University of Science and Technology Beijing, Beijing 100083, P. R. China*

Yong Luo − *Beijing Key Laboratory for Bioengineering and Sensing Technology, School of Chemistry and Biological Engineering, University of Science and Technology Beijing, Beijing 100083, P. R. China*

Conghui Liu − *School of Biomedical Engineering, Shenzhen University, Shenzhen, Guangdong 518060, P. R. China;* orcid.org/0000-0003-4873-8277

Xuan Gao − *Beijing Key Laboratory for Bioengineering and Sensing Technology, School of Chemistry and Biological Engineering, University of Science and Technology Beijing, Beijing 100083, P. R. China*

Zhihao Cheng − *Beijing Key Laboratory for Bioengineering and Sensing Technology, School of Chemistry and Biological Engineering, University of Science and Technology Beijing, Beijing 100083, P. R. China*

Yongqiang Wen − *Beijing Key Laboratory for Bioengineering and Sensing Technology, School of Chemistry and Biological Engineering, University of Science and Technology Beijing, Beijing 100083, P. R. China;* orcid.org/0000-0002-1924-4166

Complete contact information is available at: https://pubs.acs.org/10.1021/acs.analchem.0c05032

Notes

The authors declare no competing financial interest.

ACKNOWLEDGMENTS

The authors acknowledge funding from the National Natural Science Foundation of China (21804007, 21890742, and 21975019), National Postdoctoral Innovative Talents Support Program of China (BX20180036), China Postdoctoral Science Foundation (2018M631332 and 2019M650479), and Basic Research Business Fund of Central Universities (FRF-TP-18-020A1, FRF-BD-19-013A, and FRF-BD-20-14A).

REFERENCES

(1) Quesada-González, D.; Merkoçi, A. *Chem. Soc. Rev.* **2018**, *47*, 4697−4709.
(2) Zhang, L.; Ding, B.; Chen, Q.; Feng, Q.; Lin, L.; Sun, J. *Trends Anal. Chem.* **2017**, *94*, 106−116.
(3) Vashist, S. K.; Luppa, P. B.; Yeo, L. Y.; Ozcan, A.; Luong, J. H. T. *Trends Biotechnol.* **2015**, *33*, 692−705.
(4) Dincer, C.; Bruch, R.; Kling, A.; Dittrich, P. S.; Urban, G. A. *Trends Biotechnol.* **2017**, *35*, 728−742.
(5) Syedmoradi, L.; Daneshpour, M.; Alvandipour, M.; Gomez, F. A.; Hajghassem, H.; Omidfar, K. *Biosens. Bioelectron.* **2017**, *87*, 373−387.
(6) Drain, P. K.; Hyle, E. P.; Noubary, F.; Freedberg, K. A.; Wilson, D.; Bishai, W. R.; Rodriguez, W.; Bassett, I. V. *Lancet Infect. Dis.* **2014**, *14*, 239−249.
(7) Glad, C.; Grubb, A. O. *Anal. Biochem.* **1981**, *116*, 335−340.
(8) Huang, Y.; Xu, T.; Wang, W.; Wen, Y.; Li, K.; Qian, L.; Zhang, X.; Liu, G. *Microchim. Acta* **2020**, *187*, 70.
(9) Jiang, N.; Ahmed, R.; Damayantharan, M.; Unal, B.; Butt, H.; Yetisen, A. K. *Adv. Healthcare Mater.* **2019**, *8*, 1900244.
(10) Hu, J.; Wang, S.; Wang, L.; Li, F.; Pingguan-Murphy, B.; Lu, T. J.; Xu, F. *Biosens. Bioelectron.* **2014**, *54*, 585−597.
(11) Parolo, C.; Merkoçi, A. *Chem. Soc. Rev.* **2013**, *42*, 450−457.
(12) Ge, X.; Asiri, A. M.; Du, D.; Wen, W.; Wang, S.; Lin, Y. *Trends Anal. Chem.* **2014**, *58*, 31−39.
(13) Yanagisawa, N.; Dutta, D. *Anal. Chem.* **2012**, *84*, 7029−7036.
(14) Yetisen, A. K.; Akram, M. S.; Lowe, C. R. *Lab Chip* **2013**, *13*, 2210−2251.
(15) Zhang, Y.; Bai, J.; Ying, J. Y. *Lab Chip* **2015**, *15*, 1465−1471.

(16) Gonzalez, J. M.; Foley, M. W.; Bieber, N. M.; Bourdelle, P. A.; Niedbala, R. S. *Anal. Bioanal. Chem.* **2011**, *400*, 3655−3664.
(17) López Marzo, A. M.; Pons, J.; Blake, D. A.; Merkoçi, A. *Anal. Chem.* **2013**, *85*, 3532−3538.
(18) Cytiva, http://www.gelifesciences.com.cn/CNLS/jsp/Whatman/Blood%20Separator.html.web (accessed 2020.9.1).
(19) Berger, A. G.; Restaino, S. M.; White, I. M. *Anal. Chim. Acta* **2017**, *949*, 59−66.
(20) Rohrman, B.; Richards-Kortum, R. *Anal. Chem.* **2015**, *87*, 1963−1967.
(21) Huang, Y.; Wu, T.; Wang, F.; Li, K.; Qian, L.; Zhang, X.; Liu, G. *Molecule* **2019**, *24*, 2759.
(22) Huang, Y.; Wen, Y.; Baryeh, K.; Takalkar, S.; Lund, M.; Zhang, X.; Liu, G. *Microchim. Acta* **2017**, *184*, 4287−4294.
(23) Lu, X.; Liang, X.; Dong, J.; Fang, Z.; Zeng, L. *Anal. Bioanal. Chem.* **2016**, *408*, 6703−6709.
(24) Sharma, A.; Tok, A. I. Y.; Lee, C.; Ganapathy, R.; Alagappan, P.; Liedberg, B. *Sens. Actuators, B* **2019**, *285*, 431−437.
(25) Ren, W.; Mohammed, S. I.; Wereley, S.; Irudayaraj, J. *Anal. Chem.* **2019**, *91*, 2876−2884.
(26) Fang, Z.; Wu, W.; Lu, X.; Zeng, L. *Biosens. Bioelectron.* **2014**, *56*, 192−197.
(27) Xu, T.; Xu, L.-P.; Zhang, X. *Appl. Mater. Today* **2017**, *9*, 493−503.
(28) Xu, T.; Soto, F.; Gao, W.; Dong, R.; Garcia-Gradilla, V.; Magaña, E.; Zhang, X.; Wang, J. *J. Am. Chem. Soc.* **2015**, *137*, 2163−2166.
(29) Zhou, D.; Gao, Y.; Yang, J.; Li, Y. C.; Shao, G.; Zhang, G.; Li, T.; Li, L. *Adv. Sci.* **2018**, *5*, 1800122.
(30) Li, J.; Li, T.; Xu, T.; Kiristi, M.; Liu, W.; Wu, Z.; Wang, J. *Nano Lett.* **2015**, *15*, 4814.
(31) Laurell, T.; Petersson, F.; Nilsson, A. *Chem. Soc. Rev.* **2007**, *36*, 492.
(32) Xu, T.; Gao, W.; Xu, L.-P.; Zhang, X.; Wang, S. *Adv. Mater.* **2017**, *29*, 1603250.
(33) Ding, X.; Lin, S.-C. S.; Kiraly, B.; Yue, H.; Li, S.; Chiang, I.-K.; Shi, J.; Benkovic, S. J.; Huang, T. J. *Proc. Natl. Acad. Sci.* **2012**, *109*, 11105.
(34) Collins, D. J.; Morahan, B.; Garcia-Bustos, J.; Doerig, C.; Plebanski, M.; Neild, A. *Nat. Commun.* **2015**, *6*, 8686.
(35) Wu, Z.; Li, T.; Gao, W.; Xu, T.; Jurado-Sánchez, B.; Li, J.; Gao, W.; He, Q.; Zhang, L.; Wang, J. *Adv. Funct. Mater.* **2015**, *25*, 3881.
(36) Wang, W.; Castro, L. A.; Hoyos, M.; Mallouk, T. E. *ACS Nano* **2012**, *6*, 6122.
(37) Wu, Z.; Li, T.; Li, J.; Gao, W.; Xu, T.; Christianson, C.; Gao, W.; Galarnyk, M.; He, Q.; Zhang, L.; Wang, J. *ACS Nano* **2014**, *8*, 12041.
(38) Hansen-Bruhn, M.; de Ávila, B. E.-F.; Beltrán-Gastélum, M.; Zhao, J.; Ramírez-Herrera, D. E.; Angsantikul, P.; Gothelf, K. V.; Zhang, L.; Wang, J. *Angew. Chem., Int. Ed.* **2018**, *57*, 2657.
(39) Xu, T.; Luo, Y.; Liu, C.; Zhang, X.; Wang, S. *Anal. Chem.* **2020**, *92*, 7816−7821.
(40) Zhu, Q.; Xu, T.; Song, Y.; Luo, Y.; Xu, L.; Zhang, X. *Biosens. Bioelectron.* **2020**, *158*, 112185.
(41) Evander, M.; Nilsson, J. *Lab Chip* **2012**, *12*, 4667.
(42) Bruus, H. *Lab Chip* **2012**, *12*, 20.
(43) Woodside, S. M.; Bowen, B. D.; Piret, J. M. *AIChE J.* **1997**, *43*, 1727.
(44) Doinikov, A. A. *Recent Res. Dev.Acoust.* **2003**, *1*, 39.
(45) Sun, R.; Guo, J.; Sun, C.; Wang, T.; Luo, Z.; Zhang, Z.; Jiao, X.; Tang, W.; Yang, C.; Li, Y.; Min, J. *Energy Environ. Sci.* **2019**, *12*, 384−395.

https://dx.doi.org/10.1021/acs.analchem.0c05032
Anal. Chem. 2021, 93, 2996−3001